Title : **Geochemical implication of Eu isotopic ratio in anorthosite: new evidence of Eu isotope fractionation during feldspar crystallization**

The authors: Seung-Gu Lee (Korea Institute of Geoscience and Mineral Resources, Daejeon 34132, Korea, sgl@kigam.re.kr)
Tsuyoshi Tanaka (Nagoya University, gotanaka@ob4.aitai.ne.jp)
Mijung Lee. (Korea Polar Research Institute, KIOST, mjlee@kopri.re.kr)
The corresponding author is as follows;
1) Name: Seung-Gu Lee
2) Address: Geology Division, Korea Institute of Geoscience and Mineral Resources, Daejeon 34132, Korea
3) TEL : +82-42-868-3376
4) e-mail: sgl@kigam.re.kr

This manuscript has been submitted for publication in “Geosciences Journal”. Please note that, despite having undergone peer-review, the manuscript has yet to be formally accepted for publication. Subsequent versions of this manuscript may have slightly different content. If accepted in “Geosciences Journal”, the final version of this manuscript will be available via the ‘Peer-reviewed Publication DOI’ link on the right-hand side of this webpage. Please feel free to contact any of the authors; we welcome feedback.

Geochemical implication of Eu isotopic ratio in anorthosite: new evidence of Eu isotope fractionation during feldspar crystallization

Seung-Gu Lee[1*], Tsuyoshi Tanaka[2], Mi Jung Lee[3]

[1]Geology Division, Korea Institute of Geoscience and Mineral Resources, Daejeon 34132, Korea, sgl@kigam.re.kr, Researcher

[2]Department of Earth and Environmental Sciences, Nagoya University, Nagoya 464-8601, Japan, gotanaka@ob4.aitai.ne.jp, Emeritus Professor

[3]Division of Polar Earth-System Sciences, Korea Polar Research Institute, Incheon 21990, Korea, mjlee@kopri.re.kr, Researcher

Corresponding author:

Geology Division, Korea Institute of Geoscience and Mineral Resources

124 Gwahak-ro, Yuseong-gu, Daejeon 34132, Korea

Phone: +82-42-868-3376

sgl@kigam.re.kr, orcid.org/0000-0001-5215-6646

Running title: **Geochemical implication of Eu isotopic ratio in anorthosite**

ABSTRACT: Rare earth element geochemistry can provide critical information on the evolution of the crust-mantle system. Europium (Eu) exists in divalent and trivalent states, and Eu^{2+} can substitute for Ca^{2+} during plagioclase feldspar crystallization in reducing magmas. This leads to positive Eu anomaly in Ca-plagioclase-rich anorthosite derived from the mantle and negative Eu anomalies in fractionated silica-rich crustal rocks. While many studies have addressed Eu anomalies in REE data, especially in igneous rocs, almost none have evaluated ratios of Eu's two stable isotopes (^{151}Eu and ^{153}Eu) alongside Eu anomalies. Here we report systematic variation of the Eu isotopic ratio (δ^{153}Eu) from igneous rocks including anorthosite. This study detected a linear relationship between Eu anomalies and Eu isotopic ratios. Rhyolites and highly fractionated granites exhibited large negative Eu anomalies and negative δ^{153}Eu values while anorthosites exhibited large positive Eu anomalies and positive δ^{153}Eu values. In the case of the highly fractionated igneous rocks with negative Eu anomaly, the Eu isotope fractionation slope varied according to the degree of magmatic differentiation for both extrusive and intrusive rocks. Our finding reveals that Eu isotope fractionation in igneous rocks can provide new information related to magmatic differentiation and plagioclase feldspar fractional crystallization including anorthosite formation.

Key words: Eu isotope fractionation, Eu anomaly, magmatic differentiation, feldspar crystallization, anorthosite

1. INTRODUCTION

Rare earth elements (REEs) and their radiogenic isotopes (especially the ^{147}Sm-^{143}Nd and ^{138}La-^{138}Ce system) have provided critical constraints on the geochemical evolution of Earth and extra-terrestrial materials. Due to their similar chemical behavior and continuously varying atomic masses, REEs normalized to standard materials provide valuable petrogenetic information on magma evolution processes such as partial melting from the mantle-derived rocks, generalized crystallization from magma (Coryell et al., 1963; Fowler and Doig, 1983; Masuda, 1962; Shearer and Papike, 1989; Weill and Drake, 1973) and fractional crystallization (e.g., Bowen, 1928).

Most REEs exist in the trivalent (+3) state in natural systems, but Eu can exist in both divalent and trivalent states under magmatic redox conditions. Oxygen fugacity, temperature and crystallization of minerals can induce Eu anomalies in igneous rocks (Burnham et al., 2015). Positive or negative Eu anomalies in igneous rocks are generally interpreted as reflecting respective feldspar (particularly plagioclase) removal or accumulation during magma evolution with the size of the anomaly interpreted as indicating the degree of differentiation of the source magma (Fowler and Doig, 1983; Shearer and Papike, 1989; Weill and Drake, 1973). For example, extremely large positive Eu anomaly in the anorthosite reflect concentration of Eu substitution in the Ca site of plagioclase feldspar as the Ca^{2+} site in feldspar readily accepts Eu^{2+}. However, highly fractionated granite and high-silica rhyolite also exhibit large negative Eu anomalies.

The two stable isotopes of Eu, ^{151}Eu (47.81%) and ^{153}Eu (52.19%), occur in relatively similar natural abundances (Rosman and Taylor, 1998). Though ^{151}Eu decayed to ^{147}Pm by α decay with the half-life $T_{1/2}=5\times10^{18}$yr (Belli et al., 2007), ^{151}Eu can be considered as a stable isotope on Earth and solar system time scales. In addition, recently, Lee and Tanaka (2021a) reported Eu isotope fractionation due to light Eu isotope enrichment (^{151}Eu) in highly fractionated granite and high-silica rhyolite with large negative Eu anomalies. The report proposed that the heavier Eu isotope (^{153}Eu) enrichment in anorthosite exhibiting large Eu positive anomalies may reflect Ca-feldspar crystallization processes. Recent reports of REE isotope fractionation addressing Ce, Nd, Sm, Dy, Er and Yb (Moynier et al., 2006; Nakada et al., 2013; Shollenberger and Brebbecka, 2020; Hu et al., 2021) detected multiple isotope fractionation effects among these elements except in cases where natural systems host only a single isotope. This may indicate existence of δREE based on the isotope fractionation of 10 REEs with multiple isotopes except four mono-isotope REEs

No report have addressed Eu anomalies and Eu isotopic ratios in anorthosite or other forms of gabbro or volcanic rocks such as andesite and trachyte. This work describes Eu isotope ratios and Eu anomalies among both intrusive and extrusive igneous rocks including anorthosites, gabbro, andesite and trachyte, and further interprets Eu isotopic ratios among basalt, rhyolite and granitoids.

The objective in this study were to evaluate Eu isotope fractionation in terms of Eu anomalies in various kinds of igneous rocks for potential use as a geochemical tracer or petrogenetic proxy.

2. SAMPLES AND EXPERIMENTAL METHODS

2.1.Samples

In order to establish a comprehensive picture of Eu isotopic variation in igneous rocks, a total of 49 igneous rock samples were analyzed for Eu isotope ratios and REE abundances. Of these, 25 samples represented geochemical reference materials purchased from the U.S. Geological Survey (USGS) and the Geological Survey of Japan (GSJ), while the other samples consisted of anorthosites, granitoids and trachytes from Korea and Antarctica. The 25 geochemical reference materials in this study were as follows; Seven basalts (BCR2, BHVO2 and BIR1a purchased from the USGS; JB1a, JB1b, JB2 and JB3 from the GSJ), four andesites (AGV2 from USGS; JA1, JA2 and JA3 from GSJ), four rhyolites (RGM2 from USGS; JR1, JR2 and JR3 from GSJ), one diabase (W-2a from USGS), one dolerite (DNC1a from USGS), two gabbros (JGb1, JGb2 from GSJ), one syenite (STM2 from USGS), and five granites (G2 and GSP2 from USGS; JG1a, JG2 and JG3 from GSJ). The 24 rock samples from Korea and Antarctica consisted of fourteen granites and five anorthosites from Korea, and five trachytes from Antarctica. Absent a SRM trachyte, we used five trachytes from Antarctica (Table 1, see Appendices for more information).

"Table 1 is about here."

2.2.Sample preparation procedures for determination Eu isotope ratio determination

Sample digestion procedures followed an approach in Lee et al (2016). Approximately 100-200 mg of each sample powder was dissolved in a 2:1 mixture of 2-4 mL of concentrated HF (29M) and 1-2 mL of concentrated HNO_3 (16M) at ca. 160 ºC for more than 72 hours in 15 mL Savillex vials. After the addition of 0.1-0.2 mL of concentrated $HClO_4$, the dissolved sample solution was heated to dryness at ca. 180 ºC for more than 1 day. The cakes were re-dissolved in a mixture of 1 mL concentrated HCl and 0.5 mL concentrated HNO_3 and then dried ca. 160 ºC for 1 day. Sample residues were re-dissolved in 10 ml 6 M HCl as a stock solution. Of this, 0.5-1 ml was used to determine REE concentrations and the remainder was used for Eu isotope ratio determination.

Prior to Eu purification, REE concentration were measured in each sample using inductively coupled plasma mass spectrometry (ICP-MS, NexION350, Perkin Elmer) at Korea Institute of Geoscience and Mineral Resources (KIGAM). Although REE concentration have been previously determined for the 25 geochemical reference rocks (USGS, GSJ) have previously been characterized, we reanalyzed their REE abundances for comparison and to establish analytical integrity. The analyzed REE data from the geochemical standard reference material (SRM) agreed within 5-10% (Table 1).

In this study, Eu was separated from the REE fraction using 0.12 M 2-hydroxyisobutyric acid (HIBA) with the pH adjusted to ~4.60 (Lee and Tanaka, 2019, 2021b). Nuryno et al. (1998) showed that the elution time and resolution during the REE separation depend on HIBA pH. The authors recommend pH 4.6 as optimal for REE separation by HIBA column chromatography. In addition, Lee and Tanaka (2021a, 2021b) showed that incomplete Eu purification by trace amounts of Gd can interfere with Eu isotopic ratio measurement to present pseudo-fractionation effect. Extraction procedures gave yields of 99.9 ± 0.1% Eu

except in case of highly fractionated, silica-rich igneous rocks such as granite (JG2, MA10) and rhyolites (RGM2, JR series). Highly fractionated igneous rocks gave Eu yields of 98.5± 0.15%.

Most igneous rocks analyzed in this study yielded high purity Eu fractions of about 40-700 ng/mL. These Eu fractions can be used at concentration of 10 ng/mL or higher when measuring Eu isotope ratios by MC-ICP-MS after dilution with 4~7 mL of 2% HNO_3 (Table 2). Given the high recovery, most Eu fractions in this study showed only negligible Gd impurities. However, because highly fractionated igneous rocks may contain Gd, we re-performed HIBA column chromatography after drying and resuspension of initial Eu fraction.

2.3. Mass spectrometry for determination of Eu isotope ratio

Recently, Lee and Tanaka (2019, 2021b) developed a highly precise and accurate method for Eu isotopic ratio determination using a Sm spike as an internal standard in combination with standard-sample-standard bracketing mass bias correction (C-SSBIN). Lee et al. (2019) found that Eu isotopic ratio determined by C-SSBIN using Sm internal standardization in NIST3117a gave relatively accurate and precise estimates for Eu concentration down to 5ng/mL. Lee et al. (2021a, 2021b) describe optimal conditions for Eu isotope ratio measurement by MC-ICP-MS wherein ^{154}Gd exerts less than 0.1% on ^{154}Sm. We, accordingly, minimized isobaric interference using Sm from commercial ultrapure Sm_2O_3 (Alfa Aesar) as a spike for normalizing Eu isotopic measurements. We also monitored tail effects from both Gd and Sm. The separated Eu fraction showed no traces of Sm and only

data associated with a ratio of $^{154}Gd/^{154}Sm$ of 0.001 (0.1%) or less were further interpreted for degree of Eu isotope fractionation.

Eu isotopic ratios were measured in low-resolution mode with the Ni or Pt X-sampling and Ni X-skimmer cones using multicollector inductively coupled plasma mass spectrometry (MC-ICP-MS; Neptune Plus, Thermo Fisher Scientific Ltd.) in static mode with nine Faraday cups (amplifier resistor: 10^{11} ohm) at KIGAM. The instrument was tuned to achieve high sensitivity while maintaining flattened, square peaks and stable signals enough to ensure accurate measurements. The gain on each Faraday cup was monitored daily to ensure normalization of its efficiency. The isotopes ^{147}Sm(L4), ^{149}Sm(L3), ^{150}Sm(L2), ^{151}Eu(L1), ^{152}Sm(C), ^{153}Eu(H1), ^{154}Sm(H2), ^{155}Gd(H3), and ^{157}Gd(H4) were monitored simultaneously using nine Faraday cups for Sm normalization and Gd interference correction by the Gd matrix (Lee and Tanaka, 2021b, Table 1). These parameters gave ^{151}Eu and ^{154}Sm sensitivities of 80-100mV/ppb and 45-50mV/ppb, respectively. Polyatomic isotopes by Eu, Sm and Gd oxides did not appear during MC-ICP-MS analysis.

"Table 2 is about here."

Samples subjected to Eu isotope measurement by MC-ICP-MS was suspended in 2% HNO_3 prepared from 60% ultrapure HNO_3 (Merck, Darmstadt, Germany) and DIW (Milli-Q system, Millipore, Milford, USA). We used a diluted solution of NIST 3117a (10,000 μg/mL, Lot No. 120705) as an in-house standard for Eu isotope ratios. Data acquisition consisted of 1 block of 50 cycles with an integration time of 4.194 seconds and a sample aspiration rate of

80-100 μL/min. Peak centering was performed at the beginning of each analysis. A 250 s of washout time was used between sample measurements. Blanks were checked during, before, and after each sample measurement. After washing, ^{151}Eu, ^{154}Sm and ^{155}Gd in the blank solutions gave peaks of less than 0.15 mV, 0.11 mV and 0.02mV, respectively. This gives concentrations of about 6 pg/mL for each REE in acids used during column chromatography. Blank corrections subtracted each procedural blank from each REE measurement.

Operating conditions and data acquisition parameters including cup configuration followed those given in Lee and Tanaka (2021a, 2021b). We used ^{147}Sm/^{149}Sm (1.0868, Dubois et al., 1992) rather than ^{150}Sm/^{154}Sm to normalize Eu during Eu isotopic ratio determination. This gave more accurate and precise Eu isotope fractionation estimates for geological rocks subject to incomplete Eu purification and ^{154}Gd interference during ^{150}Sm/^{154}Sm normalization (Lee and Tanaka, 2021a, 2021b).

Eu isotope fractionation is represented in standard δ-notation in per mil relative to the NIST3117a Eu standard solution as follows: $\delta^{153}\text{Eu} = 1{,}000 \times [(^{153}\text{Eu}/^{151}\text{Eu}_{\text{sample}})/(^{153}\text{Eu}/^{151}\text{Eu}_{\text{NIST3117a}}) - 1]$. Lee and Tanaka (2019, 2021c) report that NIST3117a Eu standard reagent analyzed by MC-ICP-MS using Sm internal standard does not exhibit any Eu isotope fractionation regardless of Sm isotope pair used for normalization.

3. RESULTS

Table 3 lists REE abundances for USGS and GSJ SRMs analyzed in this study. Table 4 lists REE concentrations measured in igneous rocks from Korea and Antarctica including

198 anorthosites.

199

200 “Tables 3 and 4 are about here.”

201

202 Figures 1 and 2 show chondrite-normalized REE patterns for SRMs and the Korea and
203 Antarctic rock samples. Figure 1a-c shows REE patterns from extrusive rocks such as basalt,
204 andesite and rhyolite, while Fig. 1d-f shows REE patterns from intrusive rocks such as
205 gabbro and granitoids.

206

207 “Figures 1 and 2 are about here.”

208

209 Chondrite-normalized REE patterns from various kinds of igneous rocks (Figs. 1 and 2)
210 clearly show variation in the magnitude of Eu anomaly attributable to feldspar crystallization
211 during magmatic differentiation even though the samples are not cogenetic. The anorthosites
212 in Fig. 2a, in particular, exhibit a strikingly large Eu positive anomaly.

213 Table 5 lists Eu isotope ratios and the magnitude of the Eu anomaly from various kinds
214 of the igneous rocks. Table 3 also divides the samples into SRM and local igneous rocks for
215 comparison. Positive δ^{153}Eu values for the anorthosite indicated enrichment in the heavier Eu
216 (^{153}Eu) relative to the lighter Eu isotope (^{151}Eu).

217

218 “Table 5 is about here.”

219

220 **4. DISCUSSION**

221

222 This study sought to the relationship between Eu isotope fractionation and the
223 magnitude of Eu anomaly produced from feldspar crystallization during magmatic
224 differentiation. Figure 3 compares the magnitudes of Eu anomalies with δ^{153}Eu values
225 measured from the 49 samples to show Eu isotopic variation with a proxy for magma
226 differentiation. Three geochemical trends emerged from this comparison, First, δ^{153}Eu values
227 of highly fractionated granites and rhyolites attended large negative Eu anomalies, whereas
228 the anorthosites with large positive Eu anomalies showed relatively large positive δ^{153}Eu
229 values. This contrast indicates that the highly fractionated igneous rocks derived from felsic
230 magma in an upper crustal environment were enriched in the lighter Eu isotope (^{151}Eu),
231 whereas Ca-plagioclase-rich anorthosites, which derive from the mafic magma in a lower
232 crustal environment, were enriched in the heavier Eu isotope (^{153}Eu). Second, δ^{153}Eu value
233 varied systematically with magnitude of the Eu anomaly. Third, intrusive rocks (red symbols
234 in Fig. 3) showed different slopes in anomaly vs. isotopic values relative to those of extrusive
235 rocks (green and blue symbols in Fig. 3).

236 “Figure 3 is about here.”

237

The Sancheong anorthosites analyzed in this study are plagioclase accumulates consisting of more than 95% of plagioclase. The rock contains less than 5% quartz and less than 1% other minerals such as hornblende, biotite and muscovite. More than 98 % of the chemical compositions also consisted of SiO_2, Al_2O_3, CaO and Na_2O (Jeong et al. 1991; Kang et al., 1994) indicating plagioclase-rich rock. Plagioclase also exhibits an extremely large positive Eu anomaly. The positive Eu anomaly in anorthosite likely reflects substitution of Eu^{2+} for Ca^{2+} in plagioclase during differentiation of the anorthositic (primary) magma either in the upper mantle or at the lower crust.

Ismail et al. (1998) showed that isotope effects in Eu^{2+}/ Eu^{3+} exchange reaction can occur in aqueous solutions during cation exchange chromatography. These results showed enrichment in the heavier isotope ^{153}Eu is enriched in Eu^{2+}, which forms part of the Eu^{2+}/Eu^{3+} electron exchange system. Park et al. (2004) reported that the plagioclase of the Hadong-Sancheng anorthosite is characterized by a wide range of $\delta^{18}O$ values between - 4.4 and 8.2 ‰. Such value range indicates that the source magma of anorthosites was under the reduced environment. Dubinina and Borisov (2018) showed that the increasing of the CaO content in magma leaded the decreasing of ^{18}O in the melt with structural change of oxygen atoms in the melt. In natural melts, $\delta^{18}O$ has a tendency to increase from mafic to felsic rocks (Garlick, 1966). Moreover, the systematic correlation between Eu isotope fractionation and the magnitudes of Eu anomaly from the fractionated igneous rocks and anorthosites indicates that Eu isotope fractionation was closely related to magmatic differentiation processes such as feldspar fractional crystallization. Therefore, though it is difficult to compare directly the conditions in the magma with those in the aqueous solutions, the enrichment of heavier isotope ^{153}Eu in the anorthosites with large positive Eu anomaly may be explained due to

isotope effects in Eu^{2+}/Eu^{3+} electron exchange system during Ca-plagioclase accumulation in the anorthositic magma.

Another interesting feature in Figure 3 is that the trend of Eu isotope fractionation between the extrusive volcanic rocks and intrusive plutonic rocks seems to be different. Recently, Millet et al. (2016) reported that a correlation between enrichment in heavy Ti isotopes and SiO_2 content resulted from the fractional crystallization of Ti-bearing oxides. Yuan et al. (2022) also found that Zr isotope fractionation has different trend in different igneous system such as tholeiitic and alkaline series. These results indicate that isotope fractionation in heavy metal elements such as Ti and Zr should have a close relationship with the differentiation process of magma series. Although more in-depth studies are needed in the future, such different trend of the Eu isotope fractionation in intrusive and extrusive rocks may provide an important information for understanding the magma evolution in crust-mantle system.

The behavior of Eu is known to be determined by temperature and oxygen fugacity (Weill and Drake, 1973), and Eu anomalies are controlled by crystal chemistry and magmatic oxidation potential (Philpotts and Schnetler, 1968; Philpotts, 1970). Dauphas et al. (2014) showed that equilibrium iron isotope fractionation is controlled mainly by the redox and structural conditions in magma and suggested that magmatic differentiation is the main driver of Fe isotope fractionation in felsic magmas. In addition, Dauphas et al. (2014) proposed that stable isotopes from heterovalent elements, including Eu, may show isotopic variations in bulk rocks controlled by the redox and structural conditions in the magma. It means a possibility that a slight difference of the $\delta^{153}Eu$ values in the plutonic rocks and volcanic rocks may be due to the oxidation potential in the magma. Further study is needed to clarify

the relationship between Eu isotope fractionation and oxidation potential in an intrusive magmatic system.

In addition, we may need to notice for the plot of anorthosites and gabbros in Fig. 3. Anorthosite and gabbro are representative gabbroic rocks solidified through fractional crystallization from primary magma, and gabbro also has relatively large positive Eu anomaly. However, the δ^{153}Eu values of the gabbro are negative compared to those of the anorthosites. Anorthosite is a unique and enigmatic rock type in Earth system. Although gabbro and anorthosite are plutonic rocks and are included in the gabbroic rock groups, the geochemistry and mineralogy of gabbro are equivalent to those of basalt. This similarity may indicate that the trend in Eu isotope fractionation between gabbros and anorthosites is different. However, at present, the reason for the shift in Eu isotope ratio values between the plutonic rocks and volcanic rocks as well as for trend in Eu isotope fractionation between anorthosite and gabbro is uncertain and, therefore, needs further study.

5. CONCLUSION

We compared the magnitude of Eu anomaly in the chondrite-normalized REE pattern from various kinds of igneous rocks (the extrusive rocks and intrusive rocks including anorthosite) and their Eu isotope ratio from the fractionation. The anorthosites having large positive Eu anomalies show a geochemical characteristic of a heavier Eu isotope (^{153}Eu) enrichment (i.e., positive δ^{153}Eu value) whereas the rhyolites and highly fractionated granites having large negative Eu anomalies show a geochemical characteristic of a lighter Eu isotope

(^{151}Eu) enrichment (i.e., negative δ^{153}Eu value). Particularly, our results clearly showed that variation of the magnitude of Eu anomaly and Eu isotope fractionation in igneous rocks has systematic correlation, suggesting that Eu isotope fractionation in igneous rocks should be produced by feldspar crystallization during magma evolution. In addition, the Eu isotope fractionation in the highly fractionated volcanic and plutonic rocks was proceeded with different trend, implying that the Eu isotope fractionation from the intrusive and extrusive magma in the crustal environment may occur under different mechanism or geochemical environment. Anorthosite is a unique and enigmatic rock type in Earth system. Therefore, geochemical characteristic of Eu isotope fractionation in igneous rocks including anorthosite may provide a valuable information for solving the enigma of anorthosite formation in future.

ACKNOWLEDEMENTS

This work was supported by the grants from the Principal Research Fund of the Korea Institute of Geoscience and Mineral Resources (GP2020-003, GP2021-006) and the National Research Foundation of Korea (NRF) grant funded by the Korea government (MSIT) (2020R1F1A1075924, NP2020-012) to S-G. Lee. This work was also partly supported by grants from Korea Polar Research Institute Project (PE21050) to M.J. Lee.

REFERENCES

Belli, P., Bernabei, R., Cappella, F., Cerulli, R., Dai, C. J., Danevich, F.A., d'Angelo, A., Incicchitti, A., Kobychev, V. V., Nagorny, S. S., Nisi, S., Nozzoli, F., Prosperi, D., Tretyak,

V. I. and Turchenko, S. S., 2007, Search for α decay of natural Europium, Nuclear Physics A, 789, 15–19. https://doi.org/10.1016/j.nuclphysa.2007.03.001

Burnham, A. D., Berry, A. J., Halse, F. R., Schofield, P. F., Cibin, G. and Mosselmans, J. F. W., 2015, The oxidation state of europium in silicate melts as a function of oxygen fugacity, composition and temperature. Chemical Geology, 411, 248–259. https://doi.org/10.1016/j.chemgeo.2015.07.002

Bowen, N. L., 1956, The Evolution of the Igneous Rocks, Dover, New York, 332p.

Coryell, C. G., Chase, J. W. and Winchester, J. W., 1963, A procedure for geochemical interpretation of terrestrial rare-earth abundance patterns. Journal of Geophysical Research, 68, 559–566. https://doi.org/10.1029/JZ068i002p00559

Dauphas, N., Roskosz, M., Alp, E. E., Neuville, D. R., Hu, M. Y., Sio, C. K. Tissot, F. L. H., Zhao, J. L. Tissandier, L., Médard, E. and Cordier, C., 2014, Magma redox and structural controls on iron isotope variations in Earth's mantle and crust. Earth and Planetary Science Letter, 398, 127–140. https://doi.org/10.1016/j.epsl.2014.04.033

Dubinina, E. O. and Borisov, A. A. (2018) Structure and Composition Effects on the Oxygen Isotope Fractionation in Silicate Melts. *Petrology* **26**, 127–140..

Dubois, J. C., Retail, G. and Cesario, J., 1992, Isotopic analysis of rare earth elements by total vaporization of samples in thermal ionization mass spectrometry, Internal Journal of Mass Spectrometry and Ion Processes, 120, 163–317. https://doi.org/10.1016/0168-1176(92)85046-3

Fowler, A. D. and Doig, R., 1983. The significance of europium anomalies in the REE spectra of granites and pegmatites, Mont Laurier, Quebec. Geochimica et Cosmochimica Acta 47, 1131–1137. https://doi.org/10.1016/0016-7037(83)90243-0

Garlick, G. D., 1966, Oxygen Isotope Fractionation in Igneous Rocks. Earth and Planetary Science Letter, 1, 361–368.

Hu, J. Y., Dauphas, N., Tissot, F. L. H., Yokochi, R., Ireland, T. J., Zhang, Z. and Davis, A. M., 2021, Heating events in the nascent solar system recorded by rare earth element isotopic fractionation in refractory inclusions., Science Advances, 7, eabc2962. DOI: 10.1126/sciadv.abc2962

Ismail, I. M., Nomura, M. and Fujii, Y., 1998, Isotope effects of europium in ligand exchange system and electron exchange system using ion-exchange displacement chromatography, Journal of Chromatography A, 808, 185–191. https://doi.org/10.1016/S0021-9673(98)00116-2

Jeong, J-G., Kim, W-S. and Seo, B-M, 1991, Differentiation of the Plutonic Rocks in Saengcho-Myeon, Sancheong-gun: Trace Element Modelling for the Magmatic Differentiation. Journal of Mineralogical. Society of Korea, 4, 69–89 (with English abstract in Korean).

Kang, S-W., Yoo, B-Y., Ryoo, C. and Kim, Y-J., 1994, Petrochemistry of Plutons in the Hamyang-Macheon Area, Gyeongnam. Journal of Korean Earth Science Society, 15, 100–114 (with English abstract in Korean).

Lee, S-G., Asahara, Y., Tanaka, T., Lee, S. R. and Lee, T., 2013, Geochemical significance of the Rb-Sr, La-Ce and Sm-Nd isotope systems in A-type rocks with REE tetrad patterns and negative Eu and Ce anomalies: The Cretaceous Muamsa and Weolaksan granites, South Korea. Chemie der Erde, 73, 75–88. https://doi.org/10.1016/j.chemer.2012.11.008

Lee, S-G., Kim, J-K., Yang, D-Y. and Kim, J-Y., 2008a, Rare earth element geochemistry and Nd isotope composition of stream sediments, south Han River drainage basin, Korea,

Quaternary International, 176-177, 121–134.https://doi.org/10.1016/j.quaint.2007.05. 01 2

Lee, S-G., Kim, T., Tanaka, T, Lee, S-R. and Lee, J-I., 2016, Effect on the Measurement of Trace Element by Pressure Bomb and Conventional Teflon Vial Methods in the Digestion Technique. Journal of Petrological Society of Korea, 25, 1–13 (with English abstract in Korean).

Lee, S-G.. Kim, T-K , Lee, J-S. and Song, Y-H., 2006, Rb-Sr Isotope Geochemistry in Seokmodo Granitoids and Hot Spring, Gwangwha: An Application of Sr Isotope for Clarifying the Source of Hot Spring. Journal of Petrological Society of Korea, 15, 60–71 (with English abstract in Korean).

Lee, S-G., Lee, T.J. and Shin, H., 2008b, Rb-Sr age and its geochemical implication of granitoid cores from deep borehole at Pohang area, Korea, Journal of Geological Society of Korea, 44, 409–423 (with English abstract in Korean).

Lee, S-G. and Tanaka, T., 2019, Determination of Eu isotopic ratio by multi-collector inductively coupled plasma mass spectrometry using a Sm internal standard. Spectrochimica Acta: Part B, 156, 42–50. https://doi.org/10.1016/j.sab.2019.04.011

Lee, S-G. and Tanaka, T., 2021a, Eu isotope fractionation in highly fractionated igneous rocks with large Eu negative anomaly. Geochemical Journal, 55/6, e9–e17. https://doi.org/10.2343/geochemj.2.0631

Lee, S-G. and Tanaka, T., 2021b, Gd matrix effects on Eu isotope fractionation using MC-ICP-MS: Optimizing Europium isotope ratio measurements in geological rock samples. International Journal of Mass Spectrometry, 156, 42–50. https:// doi.org/ 10.1016/j.ijms.2021.116668

Lee, S-G. and Tanaka, T., 2021c, Eu isotope data of NIST3117a standard reagent for determination of Eu isotope fractionation in geological rocks using MC-ICP-MS. Data in Brief, 38, 107379, https://doi.org/10.1016/j.dib.2021.107369

Lee, Y., Cho, M., Cheong, W.S. and Yi, K., 2014, A massif-type (~1.86 Ga) anorthosite complex in the Yeongnam Massif, Korea: late-orogenic emplacement associated with the mantle delamination in the North China Craton. Terra Nova, 26, 408–416.

Masuda, A., 1962, Regularities in variation of relative abundances of lanthanide elements and attempt to analyze separation-index patterns of some minerals. Journal of Earth Sciences, Nagoya University, 10, 173–187.

McDonough, W. F. and Sun, S-S., 1995, The composition of the Earth, Chemical Geology, 120, 15–19. https://doi.org/10.1016/0009-2541(94)00140-4

Millet, M-A., Dauphas, N., Greber, N. D., Burton, K. W., Dale, C. W., Debret, B., Macpherson, C. G., Nowell, G. M. and Williams, H. M., 2016, Titanium stable isotope investigation of magmatic processes on the Earth and Moon. Earth and Planetary Science Letter, 449, 197–205. https://doi.org/10.1016/j.epsl.2016.05.039

Moynier, F., Bouvier, A., Blichert-Toft, J., Telouk, P., Gasperini, D. and Albarède, F., 2006, Europium isotopic variations in Allende CAIs and the nature of mass-dependent fractionation in the solar nebula. Geochimica et Cosmochimica Acta, 70, 4287–4294. https://doi.org/10.1016/j.gca.2006.06.1371

Nakada, R., Tanamizu, M. and Takahashi, Y., 2013, Difference in the stable isotopic fractionations of Ce, Nd, and Sm during adsorption on iron and manganese oxides and its interpretation based on their local structures. . Geochimica et Cosmochimica Acta, 121, 105–119. (https://doi.org/10.1016/j.gca.2013.07.014)

Nuryno, Huber, C. C. and Kleboth, K. (1998) Ion-Exchange Chromatography with an Oxalic Acid-α-Hydroxy-isobutric Acid Elnemt for the Separation and Quantitation of Rare-earth Elements in Manazite and Xenotime. Chromatographia, 48, 407–414.

Park. Y-R., Ko, B. and Lee, K-S., 2004, Oxygen and Hydrogen Isotope Studies of Fluid-Rock Interaction of the Hadong-Sancheong Anorthositic Rocks. Journal of Petrological Society of Korea, 13, 224–237.

Philpotts, J. A., 1970, Redox estimation from a calculation of Eu^{2+} and Eu^{3+} concentrations in natural phases. Earth and Planetary Science Letter, 9, 257–268. https://doi.org/10.1016/0012-821X(70)90036-1

Philpotts, J. A. and Schnetzler, C. C., 1968, Europium anomalies and the genesis of basalt. Chemical Geology, 3, 5–13. https://doi.org/10.1016/0009-2541(68)90009-0)

Rosman, K. J. R. and Taylor, P. D. F., 1998, Isotopic Composition of the Elements 1997, Pure and Applied Chemistry, 70, 217–236.

Shearer, C. K. and Papike, J. J., 1989, Is plagioclase removal responsible for the negative Eu anomaly in the source regions of mare basalts? Geochimica et Cosmochimica Acta, 53, 3331–3336. https://doi.org/10.1016/0016-7037(89)90113-0

Schaen, A. J., Schoene, B., Dufek, J., Singer, B. S., Eddy, M. P. Jicha, B. R. and Cottle, J. M, 2021, Transient rhyolite melt extraction to produce a shallow granitic pluton. Science Advances, 7: eabf0604. DOI: 10.1126/sciadv.abf0604

Shollenberger, Q. R. and Brennecka, G. A., 2020, Dy, Er, and Yb isotope compositions of meteorites and their components: Constraints on presolar carriers of the rare earth elements. Earth and Planetary Science Letter, 529, 115866. https://doi.org/ 10.1016/j.epsl.2019.115866

Weill, D. F., Drake, M. J., 1973, Europium Anomaly in Plagioclase Feldspar: Experimental Results and Semiquantitative Model. **Science, 180,** 1059–1060. DOI: 10.1126/science.180.4090.1059

Yuan, Y., Guo, J-L., Zong, K., Feng, L., Wang, Z., Moynier, F., Zhnag, W., Hu, Z. and Xu, H., 2022, Stable zirconium isotopic fractionation during alkaline magma differentiation: Implications for the differentiation of continental crust. Geochimica et Cosmochimica, Acta 326, 41–55. https://doi.org/10.1016/j.gca.2022.03.035

Figure Cations

Fig. 1. Chondrite (McDonough and Sun, 1995)-normalized REE pattern of standard reference materials (SRMs) of USGS and GSJ. (a), (b) and (c) are SRMs for volcanic (extrusive) rocks whereas (d), (e) and (f) are SRMs for intrusive rocks such as gabbro, diabase and granitoids. In this paper, we classified dolerite and diabase as plutonic rocks rather than volcanic rocks. The REE abundances of all SRMs were re-measured from this study (see Table A2). REE patterns by solid black dots were drawn by recommended values for each SRM from USGS and GSJ.

Fig. 2. Chondrite (McDonough and Sun, 1995)-normalized REE pattern of Korean and Antarctic igneous rocks. Except (b) trachyte, the others are all collected from Korea. Trachyte was collected from Antarctica. The REE abundances of Korean anorthosites and Antarctic trachytes were re-measured from this study. REE patterns of Korean granites are from Lee et al. (2004, 2006, 2008, 2013).

Fig. 3. (a) Variation of Eu isotope ratio according to magnitudes of Eu anomalies from igneous rocks. The error bars represent uncertainties (2SD) of the average δ^{153}Eu values from some of igneous rock samples. Lines; solid gray means no Eu anomaly in the chondrite-normalized REE pattern; black dotted means none of Eu isotope fractionation; red and blue dotted lines are correlation lines between magnitude of Eu anomaly and degree of Eu isotope fractionation (δ^{153}Eu) of the plutonic rocks and volcanic rocks, respectively. (b) is an enlarged diagram of the rectangle in (a), that is, the plots of igneous rocks with little Eu anomaly

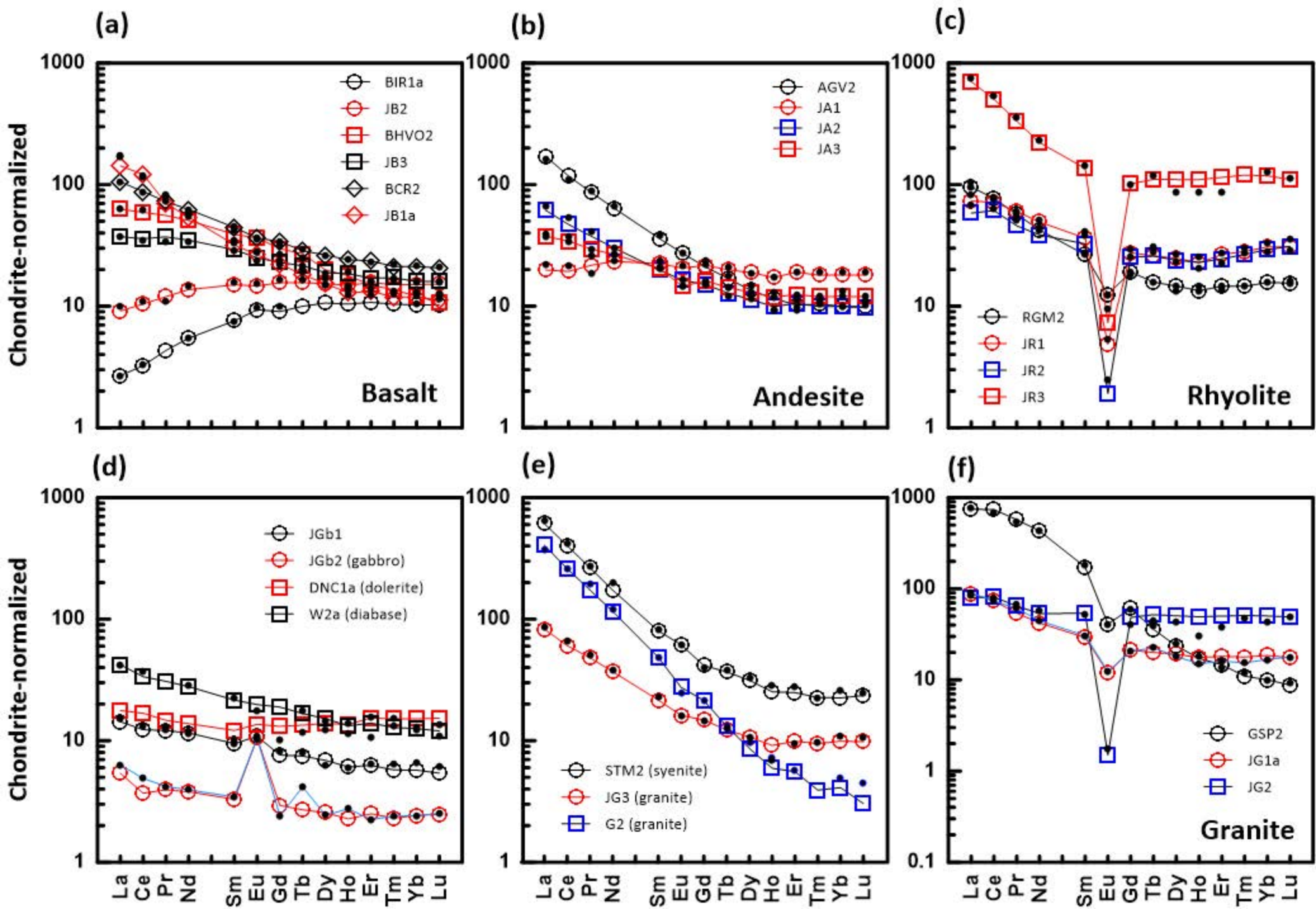
(a)
(b)
(c)
(d)
(e)
(f)
Chondrite-normalized
1000
100
10
1
0.1
BIR1a
JB2
BHVO2
JB3
BCR2
JB1a
Basalt
AGV2
JA1
JA2
JA3
Andesite
RGM2
JR1
JR2
JR3
Rhyolite
JGb1
JGb2 (gabbro)
DNC1a (dolerite)
W2a (diabase)
STM2 (syenite)
JG3 (granite)
G2 (granite)
GSP2
JG1a
JG2
Granite
La
Ce
Pr
Nd
Sm
Eu
Gd
Tb
Dy
Ho
Er
Tm
Yb
Lu

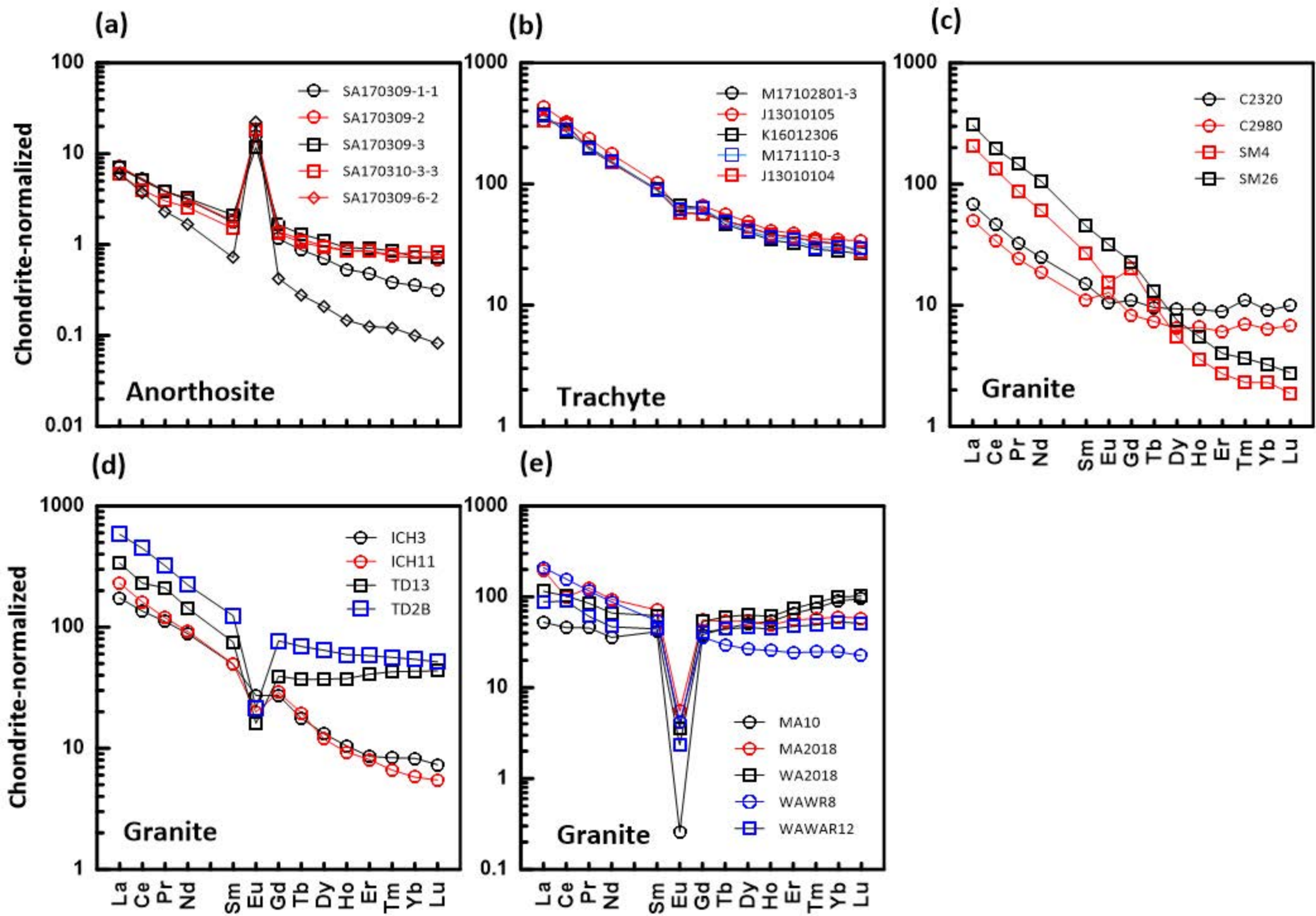
(a)
(b)
(c)
(d)
(e)
Chondrite-normalized
Chondrite-normalized
SA170309-1-1
SA170309-2
SA170309-3
SA170310-3-3
SA170309-6-2
Anorthosite
M17102801-3
J13010105
K16012306
M171110-3
J13010104
Trachyte
C2320
C2980
SM4
SM26
Granite
ICH3
ICH11
TD13
TD2B
Granite
MA10
MA2018
WA2018
WAWR8
WAWAR12
Granite
La
Ce
Pr
Nd
Sm
Eu
Gd
Tb
Dy
Ho
Er
Tm
Yb
Lu

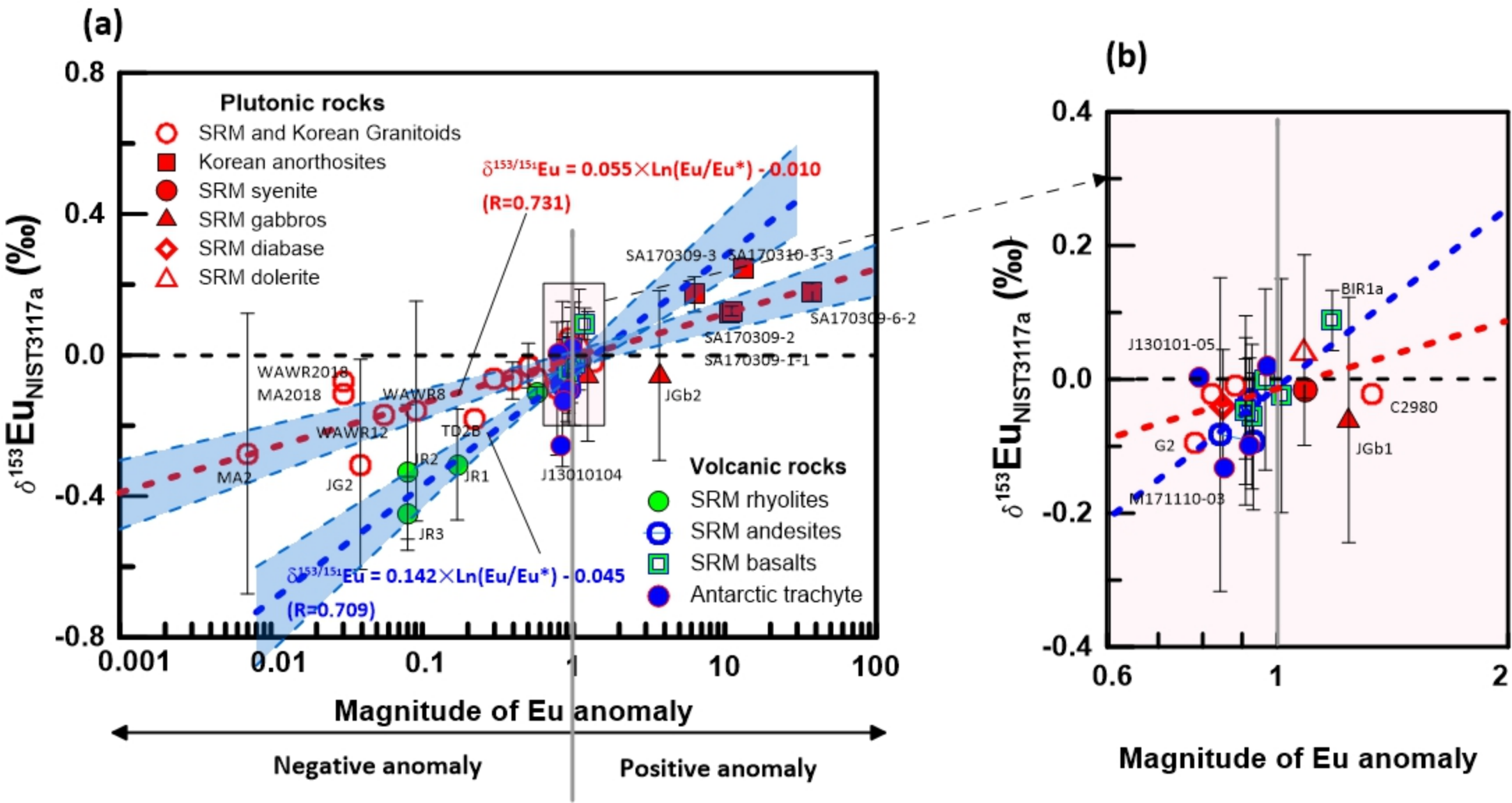
(a)
(b)
Plutonic rocks
SRM and Korean Granitoids
Korean anorthosites
SRM syenite
SRM gabbros
SRM diabase
SRM dolerite
δ153/151Eu = 0.055×Ln(Eu/Eu*) - 0.010
(R=0.731)
δ153/151Eu = 0.142×Ln(Eu/Eu*) - 0.045
(R=0.709)
Volcanic rocks
SRM rhyolites
SRM andesites
SRM basalts
Antarctic trachyte
δ153EuNIST3117a (‰)
Magnitude of Eu anomaly
Negative anomaly
Positive anomaly
WAWR2018
MA2018
WAWR8
WAWR12
MA2
JG2
TD2B
JR2
JR1
JR3
J13010104
JGb2
SA170309-3
SA170310-3-3
SA170309-6-2
SA170309-2
SA170309-1-1
BIR1a
J130101-05
C2980
G2
JGb1
M171110-03

Table 1. General information for the rock samples used in this study

Sample Name	Rock Type	Area	Location and reference	
M17102801-3	Trachyte	Mt. Melbourne (Antarctica)	74°21'16.37"S	164°44'49.81"E
J13010105			74°21'16.32"S	164°44'40.62"E
K16012306			74°20'44.53"S	164°42'28.57"E
M171110-03			74°20'43.99"S	164°45'33.29"E
J13010104			74°21'14.40"S	164°43'55.98"E
SA20170309 1-1	Anorthosite	Sancheong (Korea)	35°27'23.0"N	127°49'38.4"E
SA20170309 -2			35°27'19.5"N	127°49'33.7"E
SA20170309-3			35°26'44.2"N	127°47'23.1"E
SA20170309-6-2			35°27'15.8"N	127°48'42.4"E
SA20170310 3-3			35°27'55.0"N	127°51'41.5"E
MA2018	Granitoid	Muamsa-Weolaksan (Korea)	Lee et al. (2010, 2013)	
WA2018				
MA10				
WAWR12				
WAWR8				
SM4		Seokmodo (Korea)	Lee et al. (2006)	
SM26				
ICH3		Icheon (Korea)	Songjeong-dong, Icheon	Lee et al. (2008)
ICH11			Daecheon-ri, Icheon	
C2320		Pohang (Korea)	Lee et al. (2008a)	
C2980				
TD13		Taedo (Korea)	Lee et al. (2018)	
TD2B				

Table 2. Operating conditions for the Neptune Plus MC-ICP-MS

Instrument settings	
RF power (W)	1200
Plasma Ar gas flow rate (L/min)	16
Auxiliary Ar gas flow rate (L/min)	1
Ar carrier gas flow rate (L/min)	1.04
Sample cone	X Nickel, 1.1 mm orifice (wet plazma) Jet Nickel, 1.1 mm orifice (dry plazma)
Skimmer cone	X-cone; nickel, 0.8 mm orifice X-cone; platinum, 0.8 mm orifice
Sample uptake rate	80~100 μL/min X-cone; nickel, 0.8 mm orifice
Sample uptake Time	150 s
Wash time	250 s (Cetac ASX-110 automatic sampler), 180 s (Aridus II)
Lens settings	Optimized for maximum analyte signal intensity, □flat-topped peaks and stability
Data acquisition parameters	
Scan type	Static measurements
Cup configuration	^{147}Sm(L4), ^{149}Sm(L3), ^{150}Sm(L2), ^{151}Eu (L1), ^{152}Sm (C), ^{153}Eu (H1), ^{154}Sm (H2), ^{155}Gd (H3), ^{157}Gd (H4)
Zoom optics	Focus quad: 6 V and dispersion quad: 0 V
Sensitivity	80~100 mV/ ppb for ^{151}Eu, 45 ~ 50 mV/ ppb for ^{154}Sm, 20±2 mV/ ppb for ^{155}Gd
Integration time	4.19 sec
Number of integrations	1
Cycles/blocks or runs/passes	60

Table 3. Concentrations of Rare earth element of standard reference materials (SRMs) measured in this study

Type	Sample	La	Ce	Pr	Nd	Sm	Eu	Gd	Tb	Dy	Ho	Er	Tm	Yb	Lu	Eu/Eu*[1)]	Ref
basalt	**BCR2[2)]**	**25.0**	**53.0**	**6.80**	**28.0**	**6.70**	**2.00**	**6.80**	**1.07**	**6.41**	**1.33**	**3.66**	**0.54**	**3.50**	**0.51**	**0.90**	**USGS**
		25.0 ± 0.9 (n=4, 1σ_m)	53.7 ± 1.1 (n=4, 1σ_m)	6.73 ± 0.16 (n=4, 1σ_m)	28.5 ± 0.6 (n=4, 1σ_m)	6.58 ± 0.15 (n=4, 1σ_m)	2.05 ± 0.04 (n=4, 1σ_m)	6.76 ± 0.17 (n=4, 1σ_m)	1.03 ± 0.03 (n=4, 1σ_m)	6.48 ± 0.13 (n=4, 1σ_m)	1.32 ± 0.03 (n=4, 1σ_m)	3.77 ± 0.09 (n=4, 1σ_m)	0.52 ± 0.01 (n=4, 1σ_m)	3.41 ± 0.05 (n=4, 1σ_m)	0.51 ± 0.01 (n=4, 1σ_m)	0.94	this study
	BHVO2	**15.00**	**38.00**	**-**	**25.00**	**6.20**	**2.05**	**6.30**	**0.90**	**-**	**1.04**	**-**	**-**	**2.00**	**0.28**	**1.00**	**USGS**
		14.9 ± 0.44 (n=3, 1σ_m)	36.2 ± 1.80 (n=3, 1σ_m)	5.17 ± 0.18 (n=3, 1σ_m)	23.2 ± 1.22 (n=3, 1σ_m)	5.76 ± 0.16 (n=3, 1σ_m)	2.05 ± 0.10 (n=3, 1σ_m)	5.90 ± 0.34 (n=3, 1σ_m)	0.97 ± 0.07 (n=3, 1σ_m)	4.89 ± 0.36 (n=3, 1σ_m)	0.97 ± 0.03 (n=3, 1σ_m)	2.39 ± 0.17 (n=3, 1σ_m)	0.26 ± 0.02 (n=3, 1σ_m)	1.66 ± 0.12 (n=3, 1σ_m)	0.25 ± 0.02 (n=3, 1σ_m)	1.07	this study
	BIR1a	**0.63**	**1.90**	**-**	**2.50**	**1.10**	**0.55**	**1.80**	**-**	**4.00**	**-**	**-**	**-**	**1.70**	**0.26**	**1.13**	**USGS**
		0.64 ± 0.05 (n=3, 1σ_m)	1.99 ± 0.10 (n=3, 1σ_m)	0.40 ± 0.05 (n=3, 1σ_m)	2.49 ± 0.08 (n=3, 1σ_m)	1.12 ± 0.05 (n=3, 1σ_m)	0.53 ± 0.02 (n=3, 1σ_m)	1.80 ± 0.23 (n=3, 1σ_m)	0.36 ± 0.03 (n=3, 1σ_m)	2.61 ± 0.20 (n=3, 1σ_m)	0.57 ± 0.05 (n=3, 1σ_m)	1.72 ± 0.17 (n=3, 1σ_m)	0.34 ± 0.03 (n=3, 1σ_m)	1.94 ± 0.05 (n=3, 1σ_m)	0.26 ± 0.01 (n=3, 1σ_m)	1.13	this study
	JB1a	**37.60**	**65.90**	**7.30**	**26.00**	**5.07**	**1.46**	**4.67**	**0.69**	**3.99**	**0.71**	**2.18**	**0.33**	**2.10**	**0.33**	**0.91**	**GSJ**
		33.7 ± 0.8 (n=6, 1σ_m)	74.6 ± 9.7 (n=6, 1σ_m)	6.47 ± 0.18 (n=6, 1σ_m)	24.7 ± 0.6 (n=6, 1σ_m)	4.72 ± 0.11 (n=6, 1σ_m)	1.49 ± 0.03 (n=6, 1σ_m)	4.43 ± 0.10 (n=6, 1σ_m)	0.66 ± 0.01 (n=6, 1σ_m)	3.76 ± 0.16 (n=6, 1σ_m)	0.70 ± 0.02 (n=6, 1σ_m)	2.12 ± 0.05 (n=6, 1σ_m)	0.29 ± 0.01 (n=6, 1σ_m)	1.91 ± 0.05 (n=6, 1σ_m)	0.28 ± 0.01 (n=6, 1σ_m)	0.99	this study
	JB1b	**41.20**	**71.80**	**7.73**	**27.10**	**5.17**	**1.59**	**4.38**	**0.69**	**3.73**	**0.67**	**1.97**	**0.31**	**2.10**	**0.31**	**1.02**	**GSJ**
		40.20	70.10	7.46	26.90	4.93	1.59	5.35	0.77	4.14	0.79	2.22	0.33	2.01	0.31	0.94	this study
	JB2	**2.35**	**6.76**	**1.01**	**6.63**	**2.31**	**0.86**	**3.28**	**0.60**	**3.73**	**0.75**	**2.60**	**0.41**	**2.62**	**0.40**	**0.95**	**GSJ**
		2.18 ± 0.8 (n=8, 1σ_m)	6.39 ± 0.14 (n=8, 1σ_m)	1.11 ± 0.05 (n=8, 1σ_m)	6.26 ± 0.17 (n=8, 1σ_m)	2.22 ± 0.04 (n=8, 1σ_m)	0.83 ± 0.03 (n=8, 1σ_m)	3.09 ± 0.07 (n=8, 1σ_m)	0.56 ± 0.01 (n=8, 1σ_m)	3.77 ± 0.09 (n=8, 1σ_m)	0.81 ± 0.04 (n=8, 1σ_m)	2.51 ± 0.07 (n=8, 1σ_m)	0.37 ± 0.01 (n=8, 1σ_m)	2.42 ± 0.06 (n=8, 1σ_m)	0.37 ± 0.01 (n=8, 1σ_m)	0.96	this study
	JB3	**8.81**	**21.50**	**3.11**	**15.60**	**4.27**	**1.32**	**4.67**	**0.73**	**4.54**	**0.80**	**2.49**	**0.42**	**2.55**	**0.39**	**0.90**	**GSJ**
		8.82 ± 0.70 (n=3, 1σ_m)	22.0 ± 2.5 (n=3, 1σ_m)	3.45 ± 0.35 (n=3, 1σ_m)	16.0 ± 1.78 (n=3, 1σ_m)	4.31 ± 0.35 (n=3, 1σ_m)	1.41 ± 0.16 (n=3, 1σ_m)	4.55 ± 0.56 (n=3, 1σ_m)	0.78 ± 0.07 (n=3, 1σ_m)	4.64 ± 0.73 (n=3, 1σ_m)	1.01 ± 0.12 (n=3, 1σ_m)	2.71 ± 0.44 (n=3, 1σ_m)	0.42 ± 0.05 (n=3, 1σ_m)	2.57 ± 0.22 (n=3, 1σ_m)	0.39 ± 0.05 (n=3, 1σ_m)	0.97	this study
Rhyolite	**JR1**	**19.70**	**47.20**	**5.58**	**23.30**	**6.03**	**0.30**	**5.06**	**1.01**	**5.69**	**1.11**	**3.61**	**0.67**	**4.55**	**0.71**	**0.17**	**GSJ**
		17.35	43.83	5.58	22.52	5.37	0.27	5.48	0.94	6.09	1.25	4.25	0.70	4.94	0.76	0.15	this study
	JR2	**16.30**	**38.80**	**4.75**	**20.40**	**5.63**	**0.14**	**5.83**	**1.10**	**6.63**	**1.39**	**4.36**	**0.74**	**5.33**	**0.88**	**0.07**	**GSJ**
		13.72	37.58	4.53	17.77	4.95	0.09	5.29	0.98	6.39	1.41	4.42	0.74	5.08	0.81	0.05	this study
	JR3	**179**	**327**	**33.1**	**107**	**21.3**	**0.53**	**19.7**	**4.29**	**21.5**	**4.70**	**14.0**		**20.3**	**2.80**	**0.06**	**GSJ**
		167 ± 5 (n=4, 1σ_m)	309 ± 9 (n=4, 1σ_m)	30.9 ± 1.5 (n=4, 1σ_m)	101 ± 3 (n=4, 1σ_m)	20.1 ± 0.7 (n=4, 1σ_m)	0.41 ± 0.02 (n=4, 1σ_m)	20.2 ± 0.72 (n=4, 1σ_m)	3.99 ± 0.25 (n=4, 1σ_m)	27.1 ± 1.3 (n=4, 1σ_m)	6.00 ± 0.33 (n=4, 1σ_m)	18.3 ± 0.7 (n=4, 1σ_m)	2.96 ± 0.18 (n=4, 1σ_m)	19.0 ± 0.8 (n=4, 1σ_m)	2.71 ± 0.07 (n=4, 1σ_m)	0.06	this study
	RGM2	**25.00**	**48.00**	**5.00**	**20.00**	**4.00**	**0.70**	**3.60**	**0.60**	**3.30**	**0.80**	**2.20**			**0.40**	**0.56**	**USGS**
		22.7 ± 1.8 (n=2, 1σ_m)	47.2 ± 1.0 (n=2, 1σ_m)	5.27 ± 0.31 (n=2, 1σ_m)	19.4 ± 0.90 (n=2, 1σ_m)	3.91 ± 0.48 (n=2, 1σ_m)	0.70 ± 0.03 (n=2, 1σ_m)	3.81 ± 0.31 (n=2, 1σ_m)	0.57 ± 0.02 (n=2, 1σ_m)	3.60 ± 0.19 (n=2, 1σ_m)	0.73 ± 0.06 (n=2, 1σ_m)	2.33 ± 0.09 (n=2, 1σ_m)	0.36 ± 0.00 (n=2, 1σ_m)	0.52 ± 0.09 (n=2, 1σ_m)	0.38 ± 0.01 (n=2, 1σ_m)	0.56	this study
Andesite	**JA1**	**5.24**	**13.30**	**1.71**	**10.90**	**3.52**	**1.20**	**4.36**	**0.75**	**4.55**	**0.95**	**3.04**	**0.47**	**3.03**	**0.47**	**0.93**	**GSJ**
		4.69 ± 0.06 (n=6, 1σ_m)	11.8 ± 1.52 (n=6, 1σ_m)	2.01 ± 0.04 (n=6, 1σ_m)	10.7 ± 0.2 (n=6, 1σ_m)	3.30 ± 0.03 (n=6, 1σ_m)	1.16 ± 0.02 (n=6, 1σ_m)	4.31 ± 0.05 (n=6, 1σ_m)	0.72 ± 0.01 (n=6, 1σ_m)	4.65 ± 0.12 (n=6, 1σ_m)	0.94 ± 0.01 (n=6, 1σ_m)	3.04 ± 0.02 (n=6, 1σ_m)	0.44 ± 0.00 (n=6, 1σ_m)	2.91 ± 0.02 (n=6, 1σ_m)	0.44 ± 0.00 (n=6, 1σ_m)	0.93	this study
	JA2	**15.80**	**32.70**	**3.84**	**13.90**	**3.11**	**0.93**	**3.06**	**0.44**	**2.80**	**0.50**	**1.48**	**0.28**	**1.62**	**0.27**	**0.92**	**GSJ**
		14.5 ± 0.25 (n=6, 1σ_m)	28.8 ± 3.9 (n=6, 1σ_m)	3.48 ± 0.05 (n=6, 1σ_m)	13.8 ± 0.2 (n=6, 1σ_m)	2.93 ± 0.04 (n=6, 1σ_m)	0.92 ± 0.02 (n=6, 1σ_m)	2.99 ± 0.03 (n=6, 1σ_m)	0.46 ± 0.00 (n=6, 1σ_m)	2.78 ± 0.04 (n=6, 1σ_m)	0.54 ± 0.01 (n=6, 1σ_m)	1.69 ± 0.04 (n=6, 1σ_m)	0.25 ± 0.00 (n=6, 1σ_m)	1.59 ± 0.03 (n=6, 1σ_m)	0.24 ± 0.01 (n=6, 1σ_m)	0.95	this study
	JA3	**9.33**	**22.80**	**2.40**	**12.30**	**3.05**	**0.82**	**2.96**	**0.52**	**3.01**	**0.51**	**1.57**	**0.28**	**2.16**	**0.27**	**0.83**	**GSJ**
		8.91 ± 0.25 (n=6, 1σ_m)	21.0 ± 3.9 (n=6, 1σ_m)	2.74 ± 0.05 (n=6, 1σ_m)	12.2 ± 0.2 (n=6, 1σ_m)	3.02 ± 0.04 (n=6, 1σ_m)	0.82 ± 0.02 (n=6, 1σ_m)	3.23 ± 0.03 (n=6, 1σ_m)	0.51 ± 0.00 (n=6, 1σ_m)	3.21 ± 0.04 (n=6, 1σ_m)	0.65 ± 0.01 (n=6, 1σ_m)	1.99 ± 0.04 (n=6, 1σ_m)	0.29 ± 0.00 (n=6, 1σ_m)	1.94 ± 0.03 (n=6, 1σ_m)	0.29 ± 0.01 (n=6, 1σ_m)	0.80	this study
	AGV2	**38.00**	**68.00**	**8.30**	**30.00**	**5.70**	**1.54**	**4.69**	**0.64**	**3.60**	**0.71**	**1.79**	**0.26**	**1.60**	**0.25**	**0.91**	**USGS**
		29.3 ± 0.4 (n=6, 1σ_m)	74.6 ± 10.5 (n=6, 1σ_m)	6.26 ± 0.08 (n=6, 1σ_m)	24.2 ± 0.25 (n=6, 1σ_m)	4.39 ± 0.05 (n=6, 1σ_m)	1.41 ± 0.16 (n=6, 1σ_m)	4.55 ± 0.56 (n=6, 1σ_m)	0.78 ± 0.07 (n=6, 1σ_m)	4.64 ± 0.73 (n=6, 1σ_m)	1.01 ± 0.12 (n=6, 1σ_m)	2..71 ± 0.44 (n=6, 1σ_m)	0.42 ± 0.05 (n=6, 1σ_m)	2.57 ± 0.22 (n=6, 1σ_m)	0.39 ± 0.05 (n=6, 1σ_m)	0.96	this study
	G2	**89.0**	**160**	**18.0**	**55.0**	**7.20**	**1.40**	**4.30**	**0.48**	**2.40**	**0.40**	**0.92**	**0.18**	**0.48**	**0.11**	**0.78**	**USGS**
		96.1 ± 12.1 (n=2, 1σ_m)	160 ± 2 (n=2, 1σ_m)	16.1 ± 1.1 (n=2, 1σ_m)	53.0 ± 1.3 (n=2, 1σ_m)	7.18 ± 0.06 (n=2, 1σ_m)	1.55 ± 0.09 (n=2, 1σ_m)	4.07 ± 0.17 (n=2, 1σ_m)	0.47 ± 0.01 (n=2, 1σ_m)	2.13 ± 0.16 (n=2, 1σ_m)	0.32 ± 0.04 (n=2, 1σ_m)	0.89 ± 0.02 (n=2, 1σ_m)	0.10 ± 0.05 (n=2, 1σ_m)	0.66 ± 0.11 (n=2, 1σ_m)	0.07 ± 0.02 (n=2, 1σ_m)	0.86	this study

	GSP2	**180**	**410**	**51.0**	**200**	**27.0**	**2.30**	**12.0**	**1.40**	**6.10**	**1.00**	**2.20**	**0.30**	**1.60**	**0.23**	**0.39**	**USGS**
		176 ± 19 (n=4, 1σ_m)	453 ± 30 (n=4, 1σ_m)	53.1 ± 4.4 (n=4, 1σ_m)	197 ± 15 (n=4, 1σ_m)	25.6 ± 1.5 (n=4, 1σ_m)	2.30 ± 0.11 (n=4, 1σ_m)	12.1 ± 0.6 (n=4, 1σ_m)	1.29 ± 0.06 (n=4, 1σ_m)	5.82 ± 0.27 (n=4, 1σ_m)	0.94 ± 0.03 (n=4, 1σ_m)	2.34 ± 0.09 (n=4, 1σ_m)	0.27 ± 0.01 (n=4, 1σ_m)	1.61 ± 0.03 (n=4, 1σ_m)	0.22 ± 0.01 (n=4, 1σ_m)	0.40	this study
Granite	**JG1a**	**21.30**	**45.00**	**5.63**	**20.40**	**4.53**	**0.70**	**4.10**	**0.81**	**4.44**	**0.82**	**2.57**	**0.38**	**2.70**	**0.44**	**0.50**	**GSJ**
		20.9 ± 0.69 (n=5, 1σ_m)	45.0 ± 1.9 (n=5, 1σ_m)	5.02 ± 0.11 (n=5, 1σ_m)	19.2 ± 0.5 (n=5, 1σ_m)	4.32 ± 0.11 (n=5, 1σ_m)	0.68 ± 0.02 (n=5, 1σ_m)	4.21 ± 0.16 (n=5, 1σ_m)	0.72 ± 0.03 (n=5, 1σ_m)	4.70 ± 0.24 (n=5, 1σ_m)	0.96 ± 0.06 (n=5, 1σ_m)	2.90 ± 0.17 (n=5, 1σ_m)	0.44 ± 0.03 (n=5, 1σ_m)	2.98 ± 0.22 (n=5, 1σ_m)	0.43 ± 0.03 (n=5, 1σ_m)	0.48	this study
	JG2	**19.90**	**48.30**	**6.20**	**26.40**	**7.78**	**0.10**	**8.01**	**1.62**	**10.50**	**1.67**	**6.04**	**1.16**	**6.85**	**1.22**	**0.04**	**GSJ**
		19.0 ± 0.72 (n=4, 1σ_m)	49.6 ± 1.3 (n=4, 1σ_m)	6.00 ± 0.26 (n=4, 1σ_m)	24.4 ± 0.75 (n=4, 1σ_m)	7.97 ± 0.22 (n=4, 1σ_m)	0.08 ± 0.02 (n=4, 1σ_m)	9.63 ± 0.47 (n=4, 1σ_m)	1.87 ± 0.13 (n=4, 1σ_m)	12.4 ± 0.8 (n=4, 1σ_m)	2.69 ± 0.17 (n=4, 1σ_m)	8.01 ± 0.38 (n=4, 1σ_m)	1.26 ± 0.07 (n=4, 1σ_m)	8.11 ± 0.39 (n=4, 1σ_m)	1.21 ± 0.07 (n=4, 1σ_m)	0.03	this study
	JG3	**20.60**	**40.30**	**4.70**	**17.20**	**3.39**	**0.90**	**2.92**	**0.46**	**2.59**	**0.38**	**1.52**	**0.24**	**1.77**	**0.26**	**0.87**	**GSJ**
		19.7 ± 0.23 (n=6, 1σ_m)	37.2 ± 4.8 (n=6, 1σ_m)	4.47 ± 0.07 (n=6, 1σ_m)	16.9 ± 0.03 (n=6, 1σ_m)	3.20 ± 0.03 (n=6, 1σ_m)	0.91 ± 0.02 (n=6, 1σ_m)	2.95 ± 0.02 (n=6, 1σ_m)	0.44 ± 0.01 (n=6, 1σ_m)	2.64 ± 0.03 (n=6, 1σ_m)	0.50 ± 0.00 (n=6, 1σ_m)	1.58 ± 0.01 (n=6, 1σ_m)	0.23 ± 0.00 (n=6, 1σ_m)	1.60 ± 0.02 (n=6, 1σ_m)	0.24 ± 0.00 (n=6, 1σ_m)	0.90	this study
diabase	**W2a**	**10.00**	**23.00**	**-**	**13.00**	**3.30**	**1.00**	**-**	**0.63**	**3.60**	**0.76**	**2.50**	**0.38**	**2.10**	**0.33**	**-**	**USGS**
		10.0 ± 0.07 (n=6, 1σ_m)	20.6 ± 2.8 (n=6, 1σ_m)	2.86 ± 0.02 (n=6, 1σ_m)	12.7 ± 0.06 (n=6, 1σ_m)	3.19 ± 0.04 (n=6, 1σ_m)	1.12 ± 0.02 (n=6, 1σ_m)	3.76 ± 0.05 (n=6, 1σ_m)	0.60 ± 0.01 (n=6, 1σ_m)	3.74 ± 0.04 (n=6, 1σ_m)	0.72 ± 0.01 (n=6, 1σ_m)	2.23 ± 0.01 (n=6, 1σ_m)	0.32 ± 0.00 (n=6, 1σ_m)	2.02 ± 0.02 (n=6, 1σ_m)	0.30 ± 0.01 (n=6, 1σ_m)	0.98	this study
dolerite	**DNC1a**	**3.60**		**1.20**	**5.20**	**1.41**	**0.59**	**2.00**	**0.42**	**3.00**	**0.62**	**1.70**	**0.33**	**2.00**	**0.27**	**1.07**	**USGS**
		4.20 ± 0.39 (n=4, 1σ_m)	10.3 ± 0.9 (n=4, 1σ_m)	1.37 ± 0.12 (n=4, 1σ_m)	6.31 ± 0.57 (n=4, 1σ_m)	1.80 ± 0.17 (n=4, 1σ_m)	0.77 ± 0.08 (n=4, 1σ_m)	2.61 ± 0.25 (n=4, 1σ_m)	0.48 ± 0.04 (n=4, 1σ_m)	3.40 ± 0.25 (n=4, 1σ_m)	0.74 ± 0.03 (n=4, 1σ_m)	2.47 ± 0.22 (n=4, 1σ_m)	0.37 ± 0.03 (n=4, 1σ_m)	2.44 ± 0.20 (n=4, 1σ_m)	0.38 ± 0.03 (n=4, 1σ_m)	1.08	this study
syenite	**STM2**	**154**	**256**	**25.0**	**81.0**	**12.0**	**3.45**	**8.00**	**1.38**	**8.01**	**1.55**	**4.40**	**0.55**	**4.20**	**0.60**	**1.07**	**USGS**
		153 ± 5 (n=2, 1σ_m)	258 ± 17 (n=2, 1σ_m)	26.8 ± 0.9 (n=2, 1σ_m)	79.5 ± 7 (n=2, 1σ_m)	12.5 ± 0.3 (n=2, 1σ_m)	3.72 ± 0.08 (n=2, 1σ_m)	12.5 ± 0.1 (n=2, 1σ_m)	1.30 ± 0.28 (n=2, 1σ_m)	7.90 ± 0.11 (n=2, 1σ_m)	1.54 ± 0.07 (n=2, 1σ_m)	4.25 ± 0.05 (n=2, 1σ_m)	0.66 ± 0.04 (n=2, 1σ_m)	0.69 ± 0.13 (n=2, 1σ_m)	0.06 ± 0.00 (n=2, 1σ_m)	1.01	this study
gabbro	**JGb1**	**3.60**	**8.17**	**1.13**	**5.47**	**1.49**	**0.62**	**1.61**	**0.29**	**1.56**	**0.33**	**1.04**	**0.16**	**1.06**	**0.15**	**1.22**	**GSJ**
		3.40 ± 0.09 (n=5, 1σ_m)	7.55 ± 1.2 (n=5, 1σ_m)	1.12 ± 0.03 (n=5, 1σ_m)	5.29 ± 0.14 (n=5, 1σ_m)	1.40 ± 0.04 (n=5, 1σ_m)	0.61 ± 0.01 (n=5, 1σ_m)	1.52 ± 0.19 (n=5, 1σ_m)	0.27 ± 0.01 (n=5, 1σ_m)	1.70 ± 0.12 (n=5, 1σ_m)	0.33 ± 0.03 (n=5, 1σ_m)	1.00 ± 0.07 (n=5, 1σ_m)	0.14 ± 0.01 (n=5, 1σ_m)	0.92 ± 0.04 (n=5, 1σ_m)	0.13 ± 0.01 (n=5, 1σ_m)	1.27	this study
	JGb2	**1.50**	**3.00**	**0.39**	**1.80**	**0.51**	**0.59**	**0.48**	**0.15**	**0.60**	**0.15**	**0.36**	**0.06**	**0.39**	**0.06**	**3.63**	**GSJ**
		1.28 ± 0.13 (n=2, 1σ_m)	2.27 ± 0.42 (n=2, 1σ_m)	0.37 ± 0.01 (n=2, 1σ_m)	1.74 ± 0.04 (n=2, 1σ_m)	0.49 ± 0.01 (n=2, 1σ_m)	0.59 ± 0.00 (n=2, 1σ_m)	0.58 ± 0.06 (n=2, 1σ_m)	0.10 ± 0.03 (n=2, 1σ_m)	0.63 ± 0.02 (n=2, 1σ_m)	0.12 ± 0.01 (n=2, 1σ_m)	0.40 ± 0.02 (n=2, 1σ_m)	0.06 ± 0.00 (n=2, 1σ_m)	0.39 ± 0.00 (n=2, 1σ_m)	0.06 ± 0.00 (n=2, 1σ_m)	3.38	this study

[1)] The magnitude of Eu anomaly is defined as s the ratio Eu_N/Eu^* where Eu* is SQRT(Sm_N x Gd_N). The magnitude was calculated based on the values of Sm, Eu and Gd from the reference.

[2)] The bold number of this raw are recommended value by United States of Geological Survey (USGS) or Geological Survey of Japan (GSJ)

Table 4 . Rare earth element concentrations of igneous rocks from Korea and Antarctica used in this study

Rock Type	Area	Sample Name	La (ppm)	Ce (ppm)	Pr (ppm)	Nd (ppm)	Sm (ppm)	Eu (ppm)	Gd (ppm)	Tb (ppm)	Dy (ppm)	Ho (ppm)	Er (ppm)	Tm (ppm)	Yb (ppm)	Lu (ppm)	Eu/Eu*	Reference
Trachyte	Mt. Melbourne (Antarctica)	M17102801-3	78.42	190.5	18.12	68.07	13.17	3.26	11.29	1.80	10.81	2.10	5.79	0.83	5.14	0.66	0.81	This study
		J13010105	103.3	198.7	21.92	80.38	15.09	3.46	13.09	2.04	11.92	2.26	6.25	0.88	5.57	0.83	0.75	
		K16012306	87.78	164.8	18.74	70.02	13.35	3.76	12.51	1.68	9.89	1.88	5.19	0.71	4.50	0.65	0.89	
		M171110-03	86.93	172.4	18.10	70.93	12.98	3.49	12.50	1.77	10.11	1.99	5.58	0.73	4.88	0.72	0.84	
		J13010104	78.42	190.5	18.12	68.07	13.17	3.26	11.29	1.80	10.81	2.10	5.79	0.83	5.14	0.66	0.81	
Anorthosite	Sancheong (Korea)	SA20170309 1-1	1.64	3.25	0.36	1.41	0.26	0.87	0.23	0.03	0.17	0.03	0.08	0.01	0.06	0.01	10.83	
		SA20170309 -2	1.73	3.18	0.36	1.43	0.27	0.99	0.28	0.04	0.24	0.05	0.13	0.02	0.12	0.02	11.08	
		SA20170309-3	1.65	3.12	0.35	1.47	0.31	0.66	0.33	0.05	0.27	0.05	0.15	0.02	0.12	0.02	6.29	
		SA20170309-6-2	1.42	2.27	0.22	0.77	0.11	1.24	0.08	0.01	0.05	0.01	0.02	0.00	0.02	0.002	38.53	
		SA20170310 3-3	1.41	2.45	0.28	1.17	0.22	1.04	0.26	0.04	0.23	0.05	0.14	0.02	0.13	0.02	13.09	
Granitoid	Muamsa-Weolaksan (Korea)	MA10	12.42	28.12	4.23	16.35	6.12	0.01	7.61	1.62	12.39	2.92	10.46	1.86	14.55	2.34	0.01	Lee et al. (2013)
		WAWR12	20.97	54.60	5.67	21.40	6.56	0.13	8.13	1.59	11.35	2.41	7.57	1.21	8.54	1.25	0.05	
		MA2018	46.39	60.86	11.64	42.91	10.59	0.31	11.08	1.93	13.23	2.66	8.95	1.42	9.67	1.43	0.09	
		WA2018	27.30	62.63	7.88	30.31	9.17	0.20	10.63	2.17	15.58	3.31	11.85	2.14	16.01	2.51	0.06	
		WAWR8	49.60	96.30	10.80	40.20	8.07	0.24	7.15	1.07	6.56	1.40	3.88	0.61	3.97	0.56	0.10	
	Seokmodo (Korea)	SM4	48.70	81.50	8.11	27.70	4.00	0.87	4.00	0.36	1.35	0.20	0.44	0.06	0.37	0.05	0.66	Lee et al. (2006)
		SM26	72.80	120.80	13.50	48.50	6.66	1.78	4.55	0.47	1.85	0.30	0.64	0.09	0.52	0.07	0.99	
	Icheon (Korea)	ICH3	41.20	83.00	10.32	40.28	7.29	1.54	5.42	0.64	3.24	0.57	1.37	0.21	1.33	0.18	0.75	Lee et al. (2008a)
		ICH11	54.50	98.70	11.10	42.10	7.34	1.12	5.75	0.71	2.92	0.51	1.29	0.16	0.93	0.13	0.53	
	Pohang (Korea)	C2320	16.15	28.50	3.03	11.35	2.20	0.59	2.18	0.35	2.30	0.50	1.42	0.28	1.46	0.25	0.81	Lee et al. (2008b)
		C2980	11.95	20.93	2.24	8.49	1.64	0.72	1.65	0.27	1.58	0.36	0.97	0.17	1.03	0.17	1.33	
	Taedo (Korea)	TD13	79.97	141.0	19.52	65.33	11.11	0.90	7.83	1.33	9.16	2.05	6.54	1.06	6.96	1.07	0.30	This study
		TD2B	138.3	273.9	29.76	101.8	18.36	1.21	15.36	2.50	15.84	3.23	9.31	1.39	8.73	1.27	0.22	

Table 5. Eu isotope ratio from SRM and local igneous rocks in this study

	Extrusive (volcanic) rocks																				Intrusive (plutonic) rocks			
Rock type	**Basalt (SRM)**							**Andesite (SRM)**				Trachyte (Antarctica)						**Rhyolite (SRM)**			**Diabase**	**Dolerite**	**Gabbro (SRM)**	
Sample name	***BCR2*** [1]	**JB2**	**JB1a**	**JB2**	**JB3**	**BHVO2**	**BIR1a**	**JA1**	**JA2**	**JA3**	**AGV2**	M1710 2801-3	J1301 0105	K1601 2306	M1711 10-03	J1301 0104	**JR2**	**JR1**	**RGM2**	**JR3**	**W2a**	**DNC1a**	**JGb1**	**JGb2**
$(Eu/Eu^*)_N$ [2]	0.94	0.96	0.99	0.96	0.97	1.07	1.13	0.93	0.95	0.80	0.99	0.81	0.75	0.89	0.84	0.81	0.07	0.15	0.56	0.06	0.98	1.08	1.27	3.38
Eu concentration range (ng/mL) in the solution during MC-ICP-MS operation [3]	20~100	10~80	20~100	20~80	20~100	20~100	20~50	50~200	20~100	20~60	5~30	80	60	70	50	50	5~15	15~30	10~40	10~20	20~40	10~40	20~40	10~40
$\delta^{153/151}Eu$ [4]	***-0.08*** [5]	-0.02	-0.05	-0.02	-0.05	-0.02	0.09	-0.13	-0.09	-0.08	-0.03	0.02	0.00	-0.10	-0.13	-0.26	-0.37	***-0.28***	-0.10	-0.50	-0.04	0.04	-0.07	-0.08
2SD	0.04 (n=12)	0.14 (n=10)	0.14 (n=8)	0.14 (n=10)	0.10 (n=14)	0.17 (n=4)	0.05 (n=7)	0.20 (n=7)	0.09 (n=7)	0.23 (n=7)	0.12 (n=3)	-	-	-	-	-	-	0.08 (n=2)	0.02 (n=3)	0.27 (n=4)	0.08 (n=5)	0.14 (n=6)	0.19 (n=7)	0.23 (n=11)
$^{154}Gd^*/^{154}Sm$ [6] (%, 2SD)	0.03± 0.07	0.00± 0.01	0.01± 0.02	0.00± 0.01	0.01± 0.04	0.04± 0.09	0.02± 0.03	0.00± 0.01	0.01± 0.02	0.03± 0.06	0.00± 0.00	0.09	0.08	0.06	0.03	0.03	0.02	0.00± 0.00	0.03± 0.02	0.00± 0.00	0.04± 0.07	0.01± 0.03	0.02± 0.05	0.03± 0.05

Intrusive (plutonic) rocks

Rock type	Anorthosite					Granitoids												**Granitoids (SRM)**					
Sample name	SA1703 09-1-1	SA1703 09-2	SA1703 09-3	SA1703 09-6-2	SA1703 10-3-3	*MA10*	*MA* [4] *2018*	*WAWR 2018*	*WAWR 12*	*WAWR 8*	*SM4*	*SM26*	*ICH11*	*ICH3*	*C2320*	*C2980*	TD13	TD2B	**STM2**	**JG1a**	**G2**	**JG3**	**GSP2**	**JG2**
$(Eu/Eu^*)_N$ [2]	10.7	11.1	6.3	38.5	13.1	0.01	*0.09*	*0.06*	*0.05*	*0.10*	*0.66*	*0.99*	*0.51*	*0.75*	*0.81*	*1.33*	0.30	0.22	1.01	0.48	0.79	0.89	0.35	0.03
Eu concentration range (ng/mL) in the solution during MC-ICP-MS operation [3]	20	30~60	20~80	50~200	60	2~5	10	10	20	15~40	45	60	30	40	35	40	20	0	40~150	10~20	10~80	10~40	25~70	5~40
$\delta^{153/151}Eu$ [4]	0.12	0.12	0.17	0.18	0.24	**-0.28** [5]	***-0.11***	***-0.07***	***-0.17***	***-0.16***	***0.05***	***0.00***	***-0.03***	***-0.07***	***-0.02***	***-0.02***	-0.07	-0.18	0.00	***-0.03***	-0.10	***-0.01***	***-0.07***	***-0.31***
2SD	-	0.01 (n=2)	0.05 (n=3)	0.03 (n=3)	-	0.40 (n=2)	-	-	-	0.31 (n=4)	-	-	-	-	-	-	-	-	0.06 (n=5)	0.06 (n=13)	0.19 (n=4)	0.04 (n=10)	0.05 (n=17)	0.30 (n=6)
$^{154}Gd^*/^{154}Sm$ [6] (%, 2SD)	0.00	0.00± 0.00	0.00± 0.00	0.00± 0.00	0.00	0.01± 0.04.	0.00	0.00	0.10	0.05± 0.06	0.06	0.01	0.01	0.01	0.04	0.02	0.02	0.00	0.00± 0.00	0.02± 0.05	0.01± 0.03	0.01± 0.04	0.04± 0.07	0.00± 0.00

1) The samples of Bold character are SRMs of USGS and GSJ.

2) The magnitude of Eu anomaly is defined as s the ratio $(Eu/Eu^*)_N$ where Eu* is $SQRT(Sm_N \times Gd_N)$.

3) approximately range value (ng/mL) of Eu concentration in the sample solution diluted by 2% HNO_3 for MC-ICP-MS determination

4) Eu isotope ratio normalized by ^{147}Sm-^{149}Sm isotope pair (Lee and Tanaka, 2021a, 2021b).

5) Eu isotope data of bold Italic numbers re-calculated with data of Lee and Tanaka (2021a)

6) degree of ^{154}Gd intensity effect for ^{154}Sm (%): $^{154}Gd^*$ (calculated intensity) = measured intensity of $^{155}Gd \times 2.18$ % (abundance of ^{154}Gd)/14.8 % (abundance of ^{155}Gd) (Rosman and Taylor, 1998)

Supplementary Material for

Geochemical implication of Eu isotopic ratio in anorthosite: new evidence of Eu isotope fractionation during feldspar crystallization

Seung-Gu Lee[1*], Tsuyoshi Tanaka[2], Mi Jung Lee[3]

Correspondence to: sgl@kigam.re.kr

Samples

This study was initiated under the assumption that Eu isotope fractionation is associated with Eu anomaly during the evolution of the igneous rocks. Therefore, when selecting samples, except for anorthosite, silica concentration of igneous rocks and variation of the magnitude of their Eu anomaly were considered.

Except 25 geochemical reference materials purchased from the United States Geological Survey (USGS) and the Geological Survey of Japan (GSJ), anorthosites and granitoids from Korea and trachytes from Antarctica were collected for this study. The 25 geochemical reference materials in this study were as follows; Seven basalts (BCR2, BHVO2 and BIR1a purchased from the USGS; JB1a, JB1b, JB2 and JB3 from the GSJ), four andesites (AGV2 from USGS; JA1, JA2 and JA3 from GSJ), four rhyolites (RGM2 from USGS; JR1, JR2 and JR3 from GSJ), one diabase (W-2a from USGS), one dolerite (DNC1a from USGS), two gabbros (JGb1, JGb2 from GSJ), one syenite (STM2 from USGS), and five granites (G2 and GSP2 from USGS; JG1a, JG2 and JG3 from GSJ).

Twenty four local rock samples from Korea and Antarctica are as follows; fourteen granites and five anorthosites from Korea, and five trachytes from Antarctica. The trachytes were selected because I did not obtain SRMs.

1. A**northosites (Sancheong-Hadong, SA)**

The Sancheong-Hadong anorthosites occur in the southern Yeongnam Massif, South Korea. The anorthosites are known to be differentiated from mantle-derived parental magma during the Paleoproterozoic period (~1875 − 1863Ma) (Kwon and Jeong, 1990; Lee et al., 2014, 2017). This period is correspond to emplacement age of Proterozoic massif-type anorthosites in the world (Ashwal, 2017). The majority of primary plagioclase (An56-68) in the anorthosite was replaced by aggregates of smaller recrystallized grains (An46-54) (Lee et al., 2014). In order to measure Eu isotope ratio and REE abundances from anorthosites, we collected twenty seven rock samples from the outcrops in the Sancheong-Hadong area.

2. **Muamsa (MA)-Weolaksan (WA) granites**

The Muamsa-Weolaksan granites occur in the Hwanggangri district located in the NE margin of the metamorphic area of the Okcheon Belt, South Korea, which are highly fractionated Cretaceous granites with A-type geochemical characteristics. The Weolaksan granite is a batholith type whereas the Muamsa granite is narrow stock type. The granites are medium- to coarse-grained biotite granites, and were evolved from the granitic magma derived from the same source material (Lee et al., 2010, 2013, 2018).

We collected five granite samples from the outcrops in the Muamsa-Weolaksan area for determination of Eu isotope ratio and REE abundance.

3. **Pohang (C) granites**

The Pohang granites were collected from the core samples in the Pohang area covered with Tertiary sedimentary rocks and Cretaceous volcanic at southeastern part in the Gyeongsang Basin, South Korea. The Pohang granites were emplaced at Cretaceous age and show geochemical features that they were derived from mantle source material (Lee et al., 2008b).

We collected two granitic core samples for determination of Eu isotope ratio and REE abundance.

4. **Seokmodo (SM) granite**

Seokmodo is a small island located on the west coast of Korea and consists of the Jurassic biotite granitoids. Seokmodo is also known as the border between South Korea and North Korea (Lee et al., 2006).

We collected two granitoids for Eu isotope and REE abundance measurement.

5. **Icheon (ICH) granite**

The Icheon Jurassic granite occurs in the area which is located in the central Korean Peninsula. The northeastern part of these granite body consists of the Precambrian biotite gneiss. We selected two granite sample powders which was reported by Lee et al. (2008a) for Eu isotope and REE abundance measurement.

6. **Hataedo (TD) granite**

Hataedo is a small island, which is located in the southwestern sea (Yellow Sea) near to the Korean Peninsula. Hataedo granite occurs in the Hatedo and is Proterozoic alkali feldspar granite (Lee et al., 2021). We collected two granites by Lee et al. (2021) for Eu isotope and REE abundance measurement.

7. **Antarctic volcanic rocks**

We analyzed volcanic rocks from the Mt. Melbourne volcanic field (MMVF) in the Melbourne Province, Antarctica. They represent one of the most extensive volcanic provinces in the world, comparable to the alkali volcanic rocks in the East African rift systems. The McMurdo Volcanic Group is divided into three provinces: Hallett, Melbourne, and Erebus. The Melbourne province includes the three large stratovolcanoes of Mt. Overlord, The Pleiades and Mt. Melbourne which are composed of a wide range of intermediate and felsic alkali differentiates evolved from alkali basaltic rocks. The Mt. Melbourne (74.35° S; 164.70° E) is a 2732m high alkaline stratovolcano composed of scoria cones, domes, lava flows and various pyroclastic deposits (Wörner and Viereck, 1989; Giordano et al., 2012).

In this study, we collected five trachytes from Mt. Melbourne, and analysed their Eu isotope ratios and REE abundances.

Supporting Online References

Ashwal, L. D. and Bybee, G. M., 2017, Crustal evolution and temporality of anorthosites. Earth-Sciences Review, 173, 307–330.

Giordano, G., Lucci, F., Phillips, D., Cozzupoli, D. and Runci, V., 2012, Stratigraphy, geochronology and evolution of the Mt. Melbourne volcanic field (North Victoria Land, Antarctica). Bulletin of Volcanology, 74, 1985–2005.

Kwon, S. T. and Jeong, J. G., 1990, Preliminary Sr-Nd study of the Hadong-Sancheong anorthositic rocks in Korea: Implication for their origin and for the Precambrian Tectonics. Journal of Geological Society of Korea, 26, 341–349.

Lee, B. C., Kee, W-S., Byun, U. H. and Kim, S. W., 2021, Statherian (ca. 1714-1680 Ma) Extension-Related Magmatism and deformation in the Southwestern Korean Peninsula and Its Geological Significance: Constraints from the Petrological, Structural, Geochemical and Geochronogical studies of Newly Identified Granitoids, Minerals, 11, 557. https://doi.org/10.3390/min11060557.

Lee, S-G., Shin, C. S., Kim, K. H., Lee, T. J., Koh, H. J. and Song, Y. S., 2010, Petrogenesis of three Cretacous granites in the Okcheon Metamorphic Belt, South Korea: Geochemical and Nd-Sr-Pb isotopic constraints, Gondwana Research, 17, 87–101.

Lee, S-G., Ahn, I.S., Asahara, Y., Tanaka, T. and Lee, S. R., 2018, Geochemical interpretation of magnesium and oxygen isotope systematics in granites with the REE tetrad effect. Geosciences Journal, 22, 697–710.

Lee, S-G., Asahara, Y., Tanaka, T., Lee, S. R. and Lee, T., 2013, Geochemical significance of the Rb–Sr, La–Ce and Sm–Nd isotope systems in A-type rocks with REE tetrad patterns and negative Eu and Ce anomalies: The Cretaceous Muamsa and Weolaksan granites, South Korea. Chemie Der Erde, 73, 75–88.

Lee, S-G., Kim, J-K., Yang, D-Y. and Kim, J-Y., 2008a, Rare earth element geochemistry and Nd isotope composition of stream sediments, south Han River drainage basin, Korea, Quaternary International, 176-177, 121–134 .

Lee, S-G., Kim, J-K., Yang, D-Y. and Kim, J-Y., 2008a, Rare earth element geochemistry and Nd isotope composition of stream sediments, south Han River drainage basin, Korea, Quaternary. International, 176-177, 121–134.

Lee, S-G., Lee, T. and Shin, H., 2008b, Rb-Sr age and its geochemical implication of granitoid cores from deep borehole at Pohang area, Korea, Journal of Geological Society of Korea, 44, 409–423 (with English abstract in Korean).

Lee, S-G., Kim, T-K., Lee, J-S., Song, Y-H., 2006, Rb-Sr Isotope Geochemistry in Seokmodo Granitoids and Hot Spring, Gwangwha: An Application of Sr Isotope for Clarifying the Source of Hot Spring. Journal of Petrological Society of Korea 15, 60–71, (with English abstract in Korean).

Lee, Y., Cho, M., Cheong, W.S. and Yi, K., 2014, A massif-type (~1.86 Ga) anorthosite complex in the Yeongnam Massif, Korea: late-orogenic emplacement associated with the mantle delamination in the North China Craton. Terra Nova, 26, 408–416.

Lee, Y., Cho, M. and Yi, K., 2017, In situ U-Pb and Lu-Hf isotopic studies of zircons from the Sancheong-Hadong AMCG suite, Yeongnam Massif, Korea: Implications for the petrogenesis of ~1.86 Ga massif-type anorthosite. Journal of Asian Earth Sciences, 138, 629–646.

Wörner, G. and Viereck, L., 1989, The Mt. Melbourne Volcanic Field (Victoria Land, Antarctica). I. Field Observations. Geologisches Jahrbuch, 38, 369–393.